

## Voigt effect in diluted magnetic semiconductors: $\text{Cd}_{1-x}\text{Mn}_x\text{Te}$ and $\text{Cd}_{1-x}\text{Mn}_x\text{Se}$

Eunsoon Oh, D. U. Bartholomew,\* and A. K. Ramdas  
*Department of Physics, Purdue University, West Lafayette, Indiana 47907*

J. K. Furdyna and U. Debska  
*Department of Physics, University of Notre Dame, Notre Dame, Indiana 46556*  
(Received 8 April 1991)

We report a giant Voigt effect in diluted magnetic semiconductors  $\text{Cd}_{1-x}\text{Mn}_x\text{Te}$  and  $\text{Cd}_{1-x}\text{Mn}_x\text{Se}$  and present an excitonic model that describes its dispersion and  $M^2$  dependence,  $M$  being the magnetization. We discuss the Voigt effect in  $\text{Cd}_{1-x}\text{Mn}_x\text{Te}$  ( $0.10 < x < 0.45$ ), a zinc-blende diluted magnetic semiconductor, in the context of this model. In addition, we present experimental results for the Voigt effect in  $\text{Cd}_{1-x}\text{Mn}_x\text{Se}$  ( $x=0.26$  and  $0.31$ ), a diluted magnetic semiconductor with wurtzite structure, where the effect is considerably more complicated due to its lower symmetry. Specifically, we present a striking anisotropy of the Voigt effect in  $\text{Cd}_{1-x}\text{Mn}_x\text{Se}$ , which depends on the relative orientation of the applied magnetic field with respect to the optic ( $\hat{c}$ ) axis of the crystal.

### I. INTRODUCTION

Voigt effect<sup>1</sup> is the double refraction induced in a medium by an external magnetic field  $\mathbf{H}$  so that in an otherwise optically isotropic medium light polarized perpendicular to  $\mathbf{H}$  travels with a velocity different from that polarized parallel to  $\mathbf{H}$ . This phenomenon is closely related to the Faraday effect associated with the circular double refraction experienced by light traveling along  $\mathbf{H}$  in such a medium. The Voigt effect is usually very small except for photon energies very close to the band gap. In II-VI based diluted magnetic semiconductors<sup>2</sup> (DMS alloys), however, it is expected to be much larger than in nonmagnetic semiconductors, due to the very large Zeeman splittings of electronic bands in these materials (which also underlies the "giant" Faraday rotation<sup>3</sup>).

In this paper, we report the observation of a "giant" Voigt effect in  $\text{Cd}_{1-x}\text{Mn}_x\text{Te}$ , a DMS alloy having a zinc-blende structure, as well as in  $\text{Cd}_{1-x}\text{Mn}_x\text{Se}$ , a uniaxial crystal having a wurtzite structure. In the latter case, a striking anisotropy of the Voigt effect is observed, depending on the orientation of  $\mathbf{H}$  relative to the hexagonal axis of  $\text{Cd}_{1-x}\text{Mn}_x\text{Se}$ .

### II. EXPERIMENT

The samples used in our measurements were single crystals grown by the vertical Bridgman method. The samples in the form of plane-parallel wafers were polished using successively finer grits down to  $0.05 \mu\text{m}$ , and their manganese concentrations ( $x$ ) were determined by electron-probe microanalysis. These samples were placed in a variable-temperature optical cryostat equipped with a superconducting coil. White light from an incandescent lamp was sent through the sample and an external magnetic field  $\mathbf{H}$  was applied perpendicular to the wave vector of the light,  $\mathbf{k}$  (i.e., in the plane of the sample).

The light incident on the sample was linearly polarized,

with the electric field of the light at an angle of  $45^\circ$  to the magnetic field, so that the components of the electric field along and perpendicular to  $\mathbf{H}$  were equal in magnitude. Since these two components travel with different velocities, they emerge from the sample with a phase difference and the transmitted light thus becomes elliptically polarized, the elliptical polarization depending on the phase difference experienced by the two polarization components. The phase difference  $\phi$  is given by

$$\phi = \frac{El}{\hbar c} (n_{\perp} - n_{\parallel}), \quad (1)$$

where  $E$  is the photon energy,  $l$  is the thickness of the medium that the light traversed,  $c$  and  $\hbar$  have their usual meanings, and  $n_{\perp}$  and  $n_{\parallel}$  are the indices of refraction for the electric field perpendicular and parallel to  $\mathbf{H}$ , respectively. The transmitted beam passed through a linear polarizer, which was at  $-45^\circ$  with respect to  $\mathbf{H}$ . It is easily seen that in this configuration the transmitted intensity displays maxima for  $\phi = (2p+1)\pi$  and minima for  $\phi = 2p\pi$ ,  $p$  being an integer.

In Fig. 1 we show a transmission curve obtained in this manner for  $\text{Cd}_{1-x}\text{Mn}_x\text{Te}$ ,  $x=0.35$ , at a temperature  $T=20$  K,  $H=60$  kG, the spectral analysis being performed on a double monochromator. Each successive maximum or minimum corresponds to an additional increase or decrease of  $\phi$  by  $2\pi$ . In this manner, one can determine the *relative* dispersion of the Voigt effect as a function of photon energy. The *absolute* value of the Voigt effect can be determined by increasing magnetic field from 0 to 60 kG at any specific wave number. Figure 2 is such a transmission curve obtained with  $\text{Cd}_{1-x}\text{Mn}_x\text{Te}$ ,  $T=20$  K,  $\bar{\nu}=16500 \text{ cm}^{-1}$ . The Voigt effect (i.e.,  $\phi$ ) is zero for  $H=0$ , and each successive minimum indicates an increase of  $\phi$  by  $2\pi$ . Note that the period decreases with increasing magnetic field since—as we will see—the magnitude of the Voigt effect is proportional to the *square* of the external magnetic field.

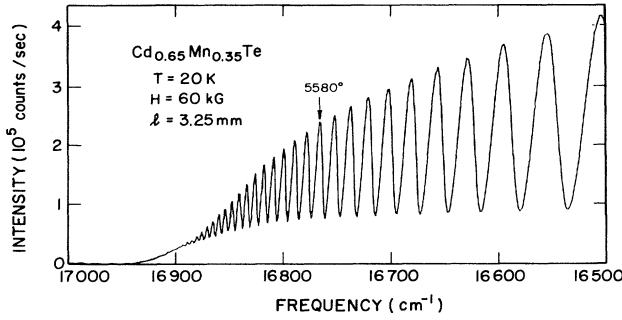


FIG. 1. Transmission of  $\text{Cd}_{1-x}\text{Mn}_x\text{Te}$ ,  $x=0.35$ ,  $T=20$  K,  $H=60$  kG, in the Voigt geometry ( $\mathbf{H}\perp\hat{\mathbf{k}}$ ). The sample is placed between two crossed polarizers at  $\pm 45^\circ$  with respect to  $\mathbf{H}$ . The intensity maxima correspond to  $\phi=(2p+1)\pi$ ,  $p$  being integers. Each successive maximum or minimum thus indicates an additional increase or decrease of  $\phi$  by  $2\pi$ .

### III. THEORY

In order to develop a model for the Voigt effect in DMS alloys, it is useful to consider the electronic band structure of  $\text{Cd}_{1-x}\text{Mn}_x\text{Te}$ . Figure 3(a) shows a schematic diagram of the band structure for the conduction-band minimum and the topmost valence-band maximum of  $\text{Cd}_{1-x}\text{Mn}_x\text{Te}$  at the zone center, in the presence of an external field  $\mathbf{H}$ . The bottom of the conduction band lies at the center of the Brillouin zone with  $\Gamma_6$  symmetry, and the top of the valence band is also at the zone center with the fourfold degenerate  $\Gamma_8$  symmetry. The spin degeneracies are lifted by the external magnetic field. There are four allowed  $\hat{\sigma}_\pm$  transitions (labeled 1,3,4,6) and two  $\hat{\pi}$  transitions (labeled 2, 5) from the  $\Gamma_8$  valence band to the  $\Gamma_6$  conduction band; the  $\hat{\sigma}_\pm$  transitions correspond to circularly polarized photons in the plane perpendicular to  $\mathbf{H}$  with polarizations given by  $\hat{\sigma}_\pm=(1/\sqrt{2})(\hat{\mathbf{x}}\pm i\hat{\mathbf{y}})e^{-i\omega t}$  for  $\mathbf{H}\parallel\hat{\mathbf{z}}$ , whereas the  $\hat{\pi}$  transitions are linearly polarized along  $\mathbf{H}$  (i.e.,  $\hat{\mathbf{z}}e^{-i\omega t}$ ). The band structure of the wurtzite  $\text{Cd}_{1-x}\text{Mn}_x\text{Se}$  differs from that of  $\text{Cd}_{1-x}\text{Mn}_x\text{Te}$  by the

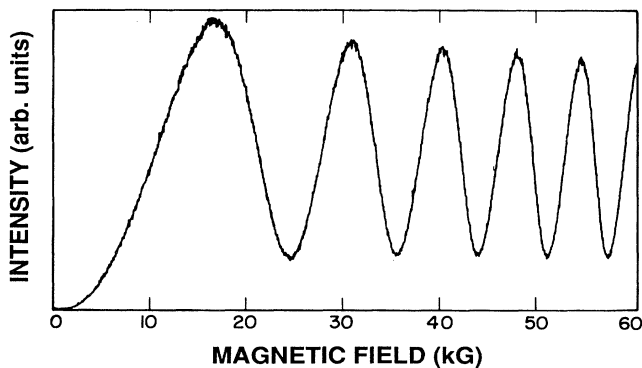


FIG. 2. Transmitted intensity vs  $H$ , showing the magnetic-field dependence of the Voigt effect for  $\text{Cd}_{1-x}\text{Mn}_x\text{Te}$ ,  $x=0.35$ ,  $T=20$  K,  $\bar{\nu}=16500$   $\text{cm}^{-1}$ .

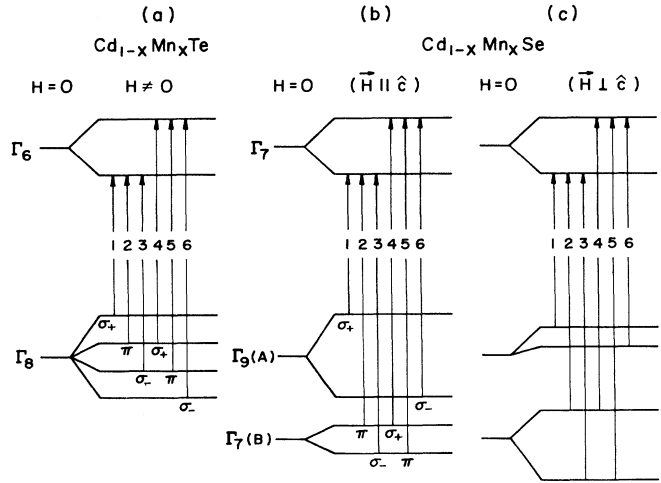


FIG. 3. A schematic diagram of the interband transitions from the valence-band maxima to the conduction-band minima in  $\text{Cd}_{1-x}\text{Mn}_x\text{Te}$  (a), in  $\text{Cd}_{1-x}\text{Mn}_x\text{Se}$  for external magnetic field ( $\mathbf{H}$ ) parallel to the optic axis  $\hat{\mathbf{c}}$  (b), and for  $\mathbf{H}$  perpendicular to  $\hat{\mathbf{c}}$  (c). [Note, for  $\mathbf{H}\perp\hat{\mathbf{c}}$  (c), these selection rules could be somewhat relaxed and may allow transitions to appear which are forbidden for  $\mathbf{H}\parallel\hat{\mathbf{c}}$ .]

crystal-field splitting associated with its uniaxial crystal structure, the Zeeman splittings now also depending on the direction of  $\mathbf{H}$  with respect to  $\hat{\mathbf{c}}$ , as shown in Figs. 3(b) and 3(c). This anisotropy of  $\text{Cd}_{1-x}\text{Mn}_x\text{Se}$  thus introduces an additional degree of complexity into the Voigt effect.

The dispersion of the refractive index  $n$  in the absence of an external magnetic field in a DMS alloy can be expressed in the form of  $n^2-1 \propto \sum f_i/(E_i^2-E^2)$ , where  $E_i$  is the energy of a specific allowed transition and  $f_i$  is the oscillator strength for that transition. For a single oscillator of energy  $E_0$ , the refractive index can be written as  $n^2=n_0^2+F_0/(E_0^2-E^2)$ , where  $F_0$  is a constant involving the oscillator strength associated with  $E_0$ , and  $n_0$  represents all contributions to  $n$  other than that associated with  $E_0$ . This form is useful when the photon energy is near  $E_0$  and far from other transition energies. In principle, any transition which exhibits Zeeman splitting in an external magnetic field will contribute to the Voigt effect, but the excitonic transitions (i.e., those nearest to the photon energies, which are below the energy gap) may be expected to dominate, as has already been observed for Faraday rotation in these alloys. The two  $\hat{\pi}$  transitions [labeled 2 and 5 in Fig. 3(a)] are significant in the dispersion of the refractive index for  $\mathbf{E}\parallel\mathbf{H}$  (i.e.,  $n_\pi=n_\parallel$ ), whereas the transitions labeled 1 and 4 (polarized in  $\hat{\sigma}_+$ ) and 3 and 6 (polarized in  $\hat{\sigma}_-$ ) together determine the dispersion of the refractive index for  $\mathbf{E}\perp\mathbf{H}$  (i.e.,  $n_\sigma=n_\perp$ ); here  $\mathbf{E}$  is the electric vector of the incident light. We also note that  $n_\parallel$  and  $n_\perp$  do not change by reversing magnetic field. In view of this the reversal of magnetic field has no effect on the birefringence, and thus the Voigt effect should behave as an even function of magnet-

ic field. At low fields the behavior of this magnetic-field-induced birefringence is thus expected to be quadratic in  $H$ . Considering the four  $\hat{\sigma}_\pm$  and the two  $\hat{\pi}$  excitonic zone center transitions from the valence band to the conduction band as shown in Fig. 3, we can express the refractive index as

$$n_\sigma^2 = n_0^2 + \sum F_i / (E_i^2 - E^2), \quad i=1,3,4,6, \quad (2a)$$

and

$$n_\pi^2 = n_0^2 + \sum F_i / (E_i^2 - E^2), \quad i=2,5, \quad (2b)$$

where  $E_i$  is an excitonic transition energy for each allowed transition, and  $F_i$  is a constant involving the oscillator strength corresponding to that transition. Note here that in the absence of an external magnetic field for an isotropic DMS (e.g.,  $\text{Cd}_{1-x}\text{Mn}_x\text{Te}$ )  $E_i = E_o$  and  $F_o = \sum F_i$ . The relative strengths of  $F_i$  are given by  $F_1:F_2:F_3:F_4:F_5:F_6 = 3:4:1:1:4:3$  (Ref. 4) for  $\text{Cd}_{1-x}\text{Mn}_x\text{Te}$ . In the case of  $\text{Cd}_{1-x}\text{Mn}_x\text{Se}$ ,  $E_i$  at  $H=0$  has two different values, namely,  $E_A$  for  $i=1,6$  and  $E_B$  for  $i=2,3,4,5$  where  $E_A$  and  $E_B$  are transition energies of the  $A$  exciton and  $B$  exciton, respectively. For  $\mathbf{H} \parallel \hat{c}$ , the quantitative analysis can be made starting from expres-

sions similar to those in Eq. (2) with the two different values of  $E_i$  at  $H=0$ . As will become clear in the following discussion, the analysis of the Voigt effect in  $\text{Cd}_{1-x}\text{Mn}_x\text{Se}$  with  $\mathbf{H} \perp \hat{c}$  needs a detailed description of the Zeeman splittings. The Voigt effect in  $\text{Cd}_{1-x}\text{Mn}_x\text{Se}$  will be discussed only qualitatively in the next section in connection with experimental results and in the remainder of this section we focus on an isotropic DMS.

We can now express the refractive indices for the  $\hat{\sigma}_\pm$  and  $\hat{\pi}$  transitions by a Taylor expansion about  $E_o$ , to the second order in  $(E_i - E_o)$ ,

$$n_\sigma^2 = n^2(0) + \sum \frac{\partial G}{\partial E} \Delta E_i + \frac{1}{2} \sum \frac{\partial^2 G}{\partial E^2} (\Delta E_i)^2, \quad i=1,3,4,6, \quad (3a)$$

$$n_\pi^2 = n^2(0) + \sum \frac{\partial G}{\partial E} \Delta E_i + \frac{1}{2} \sum \frac{\partial^2 G}{\partial E^2} (\Delta E_i)^2, \quad i=2,5, \quad (3b)$$

where  $n(0)$  is the refractive index for  $H=0$ ,  $G \equiv F_i / (E_i^2 - E^2)$ , and  $\Delta E_i$  is the excitonic Zeeman splitting of each transition energy  $(E_i - E_o)$  from 1 to 6. We thus obtain

$$\begin{aligned} n_\perp^2 - n_\parallel^2 = n_\sigma^2 - n_\pi^2 \approx & \frac{F_o E}{8(E_o^2 - E^2)^2} (3\Delta E_1 + \Delta E_3 + \Delta E_4 + 3\Delta E_6 - 4\Delta E_2 - 4\Delta E_5) \\ & + \frac{F_o (E_o^2 + 3E^2)}{16(E_o^2 - E^2)^3} [3(\Delta E_1)^2 + (\Delta E_3)^2 + (\Delta E_4)^2 + 3(\Delta E_6)^2 - 4(\Delta E_2)^2 - 4(\Delta E_5)^2]. \end{aligned} \quad (4)$$

We now note that  $\Delta E_5 = -\Delta E_2$ ,  $\Delta E_6 = -\Delta E_1$ , and  $\Delta E_4 = -\Delta E_3$ , and thus all the first-order terms in Eq. (4) vanish, leaving  $F_o (E_o^2 + 3E^2) / 8(E_o^2 - E^2)^3 [3(\Delta E_1)^2 + (\Delta E_3)^2 - 4(\Delta E_2)^2]$ . (Note that  $\Delta E_5 \neq -\Delta E_2$ , etc. for  $\mathbf{H} \perp \hat{c}$  in  $\text{Cd}_{1-x}\text{Mn}_x\text{Se}$ , and the quantitative description becomes complex for this geometry.) Let  $n_\perp - n_\parallel = (1/2n)(n_\perp^2 - n_\parallel^2)$ , where  $n = (n_\perp + n_\parallel)/2$ . For  $E$  close to  $E_o$  we can assume that  $n^2 \approx F_o / (E_o^2 - E^2)$ , and from Eq. (4) we obtain

$$\begin{aligned} n_\perp - n_\parallel \approx & \frac{(F_o)^{1/2} (E_o^2 + 3E^2)}{16(E_o^2 - E^2)^{5/2}} \\ & \times [3(\Delta E_1)^2 + (\Delta E_3)^2 - 4(\Delta E_2)^2]. \end{aligned} \quad (5)$$

As shown in Fig. 3(a), in the presence of  $\mathbf{H}$  the  $\Gamma_6$  conduction-band minimum splits into two levels, given by  $E_g \pm 3A$  and the  $\Gamma_8$  valence-band maximum into four levels given by  $\pm B$  and  $\pm 3B$ , where the energy of the valence band at  $H=0$  is taken as 0, and

$$A = \frac{1}{6} \alpha \frac{M}{g_{\text{Mn}} \mu_B}, \quad B = \frac{1}{6} \beta \frac{M}{g_{\text{Mn}} \mu_B},$$

$\alpha$  and  $\beta$  are the exchange integrals for the conduction- and valence-band electrons,  $M$  is the magnetization per unit volume, and  $g_{\text{Mn}}$  is the Landé  $g$  factor of the  $\text{Mn}^{2+}$

spins ( $g_{\text{Mn}}=2$ ). The energies of the associated excitonic transitions [which determine Eq. (5)] are  $\Delta E_1 = -3A + 3B$ ,  $\Delta E_2 = -3A + B$ , and  $\Delta E_3 = -3A - B$ ,  $B$  being negative. We then finally have

$$\phi = \frac{l}{24\hbar c} \frac{(F_o)^{1/2} E (E_o^2 + 3E^2)}{(E_o^2 - E^2)^{5/2}} \left( \frac{M}{g_{\text{Mn}} \mu_B} \right)^2 \beta (\beta - \alpha). \quad (6)$$

The magnetization  $M$  of DMS alloys in the paramagnetic state is proportional to the external magnetic field  $H$  at sufficiently low fields and/or at sufficiently high temperatures. In this regime, the Voigt effect is proportional to  $H^2$  and we can define a new parameter, representing  $\phi$  per unit length per unit square of the magnetic field, denoted by  $\Upsilon$  (in analogy with the Verdet constant used to describe the Faraday rotation) such that  $\phi = \Upsilon l H^2$ .

## IV. RESULTS AND DISCUSSIONS

### A. $\text{Cd}_{1-x}\text{Mn}_x\text{Te}$

Figure 1 shows the transmission spectrum for  $\text{Cd}_{1-x}\text{Mn}_x\text{Te}$ ,  $x=0.35$ ,  $T=20$  K,  $H=60$  kG,  $l=3.25$  mm, with the sample placed between a polarizer and an

analyzer making an angle of  $+45^\circ$  and  $-45^\circ$ , respectively, with an external magnetic field  $\mathbf{H}$ , which is in the plane of the sample, (i.e., perpendicular to the direction of propagation). As can be seen, a series of oscillations occurs as a consequence of the magnetic-field-induced birefringence and the resulting variation in  $\phi$ . The transmission maxima correspond to  $\phi = (2p + 1)\pi$ , as discussed in the preceding section. The decreasing amplitude of oscillations for increasing photon energy is in part due to the differential near-gap absorption for the electric field component polarized parallel and perpendicular to  $\mathbf{H}$ . Near the absorption edge the Voigt phase shift  $\phi$  is about  $10\,000^\circ$ , much larger than for any nonmagnetic semiconductor, arising from the huge Zeeman splittings of the excitonic transitions in the DMS's.

In Fig. 4, we show the parameter  $\Upsilon$  as a function of photon energy for a series of  $\text{Cd}_{1-x}\text{Mn}_x\text{Te}$  samples ( $x=0.13, 0.22, 0.35,$  and  $0.41$ ) at various temperatures, where  $\Upsilon$  is the Voigt phase shift  $\phi$  per  $\text{G}^2$  per cm. In order to bring out the  $M^2$  dependence on  $x$  in the Voigt effect, we compare  $\Upsilon$  at a given value of  $(E/E_0)$ ,  $E_0$  being the excitonic energy. As can be seen from the limited number of compositions studied, the Voigt effect at a given value of  $(E/E_0)$  appears to increase with increasing  $x$  up to a certain value of  $x$ , beyond which it decreases. [In the figure we identify  $(E/E_0) \approx 0.96$  at 5 K for each  $x$ .] This behavior is similar to that of the Faraday effect in  $\text{Cd}_{1-x}\text{Mn}_x\text{Te}$  or  $\text{Cd}_{1-x}\text{Mn}_x\text{Se}$ , where the Faraday rotation (or, equivalently, the magnetization) at 5 K increases up to  $x=0.25$ , beyond which it decreases.<sup>5,6</sup> This

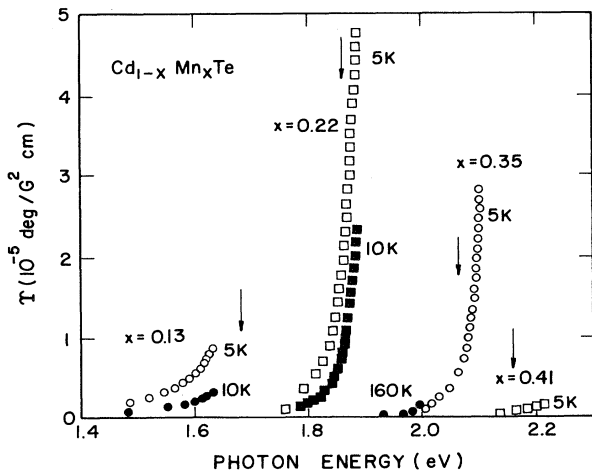


FIG. 4. The magnetic-field-induced phase difference due to the Voigt effect  $\phi$  per unit length per unit square magnetic field (designated by the parameter  $\Upsilon$ ) as a function of photon energy for  $\text{Cd}_{1-x}\text{Mn}_x\text{Te}$  ( $x=0.13, 0.22, 0.35,$  and  $0.41$ ) at various temperatures. Note the marked increase in  $\Upsilon$  close to the absorption edge for a given  $x$ . These curves indicate that the number of manganese ions ( $\text{Mn}^{2+}$ ) that can contribute to the magnetization decreases noticeably above  $x \approx 0.25$  at 5 K due to large antiferromagnetic interaction between the nearest-neighbor  $\text{Mn}^{2+}$ . The arrows identify the photon energy for  $(E/E_0) \approx 0.96$  at 5 K.

can be traced to the antiferromagnetic coupling between nearest-neighbor  $\text{Mn}^{2+}$  ions. As the temperature increases, the  $x$  value at which the peak in the Voigt effect (or the Faraday effect) occurs also increases beyond  $x=0.25$ , since the antiferromagnetic interaction is gradually becoming less important. We note that the Voigt effect depends on  $x$  more strongly than does the Faraday effect, since it depends on  $M^2$ , while the Faraday effect is linearly proportional to  $M$ .

As mentioned earlier, Fig. 2 displays the variation in the transmission of  $\text{Cd}_{1-x}\text{Mn}_x\text{Te}$ ,  $x=0.35$ ,  $T=20$  K, as the magnetic field is increased from 0 to 60 kG at a specific photon energy  $\tilde{\nu}=16\,500\text{ cm}^{-1}$ . The decreasing amplitude with increasing magnetic field is probably due to the differential absorption for the polarizations  $\parallel$  and  $\perp \mathbf{H}$ . The  $H^2$  dependence of the Voigt effect is demonstrated in Fig. 5, obtained from the data shown in Fig. 2. The magnetization of DMS alloys follows the Brillouin function  $B_{5/2}(H/(T+T_{AF}))$  in the low-temperature regime (where  $T_{AF}$  is a phenomenological measure of the Mn-Mn antiferromagnetic interactions), and thus exhibits a saturation effect for low temperatures and at high fields. This saturation effect has been extensively studied in the Faraday effect of  $\text{Cd}_{1-x}\text{Mn}_x\text{Te}$  (Ref. 5). A similar saturation in the Voigt effect is apparent in Fig. 6 for  $\text{Cd}_{1-x}\text{Mn}_x\text{Te}$ ,  $x=0.18$ ,  $T=5$  K,  $\tilde{\nu}=14\,000\text{ cm}^{-1}$ ,  $l=2.03$  mm, the figure resembling  $M^2$  as a function of  $H^2$ . Note that the saturation effect is more pronounced for the lower manganese concentrations (which have smaller  $T_{AF}$ 's). The small deviation from linearity seen in the high-field limit of Fig. 5 is an indication of the onset of the saturation of  $M$  for the  $x=0.35$  sample.

According to Eq. (6),  $\phi$  is proportional to  $E(E_0^2 + 3E^2)/(E_0^2 - E^2)^{5/2}$ . For photon energies near the band gap, the dispersion of  $\phi$  will be mainly dominated

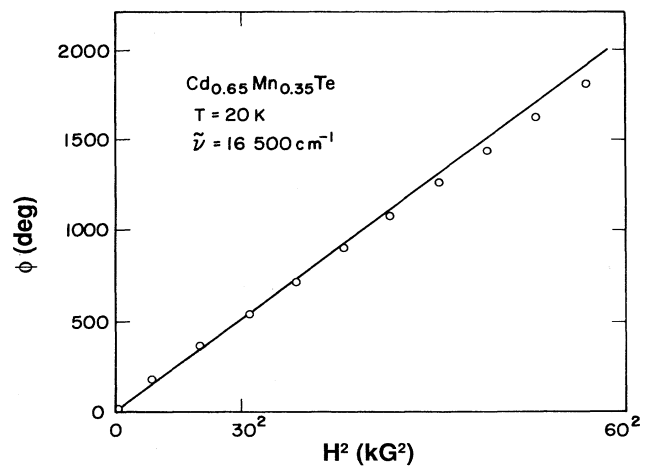


FIG. 5. The phase difference  $\phi$  between electric field parallel and perpendicular to  $\mathbf{H}$  as a function of  $H^2$ , demonstrating the  $M^2$  dependence of the Voigt effect, where  $M$  is the magnetization. The raw data are shown in Fig. 2. The small deviation at high fields from the  $H^2$  dependence is due to the saturation of the magnetization.

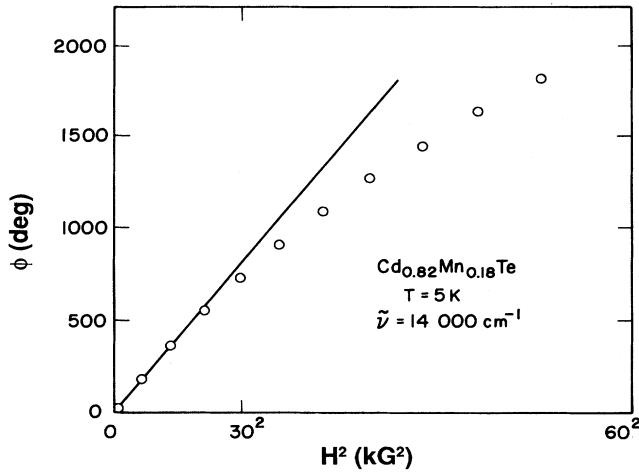


FIG. 6.  $\phi$  vs  $H^2$  for  $\text{Cd}_{1-x}\text{Mn}_x\text{Te}$ ,  $x=0.18$ ,  $T=5$  K,  $\tilde{\nu}=14000$   $\text{cm}^{-1}$ . The saturation in  $\phi$  is due to the saturation of the magnetization. For low  $x$ , low temperature, and high fields, this saturation effect is more pronounced.

by the denominator of this expression. To reveal the dependence of  $\Upsilon$  on  $E$  near the energy gap, we ignore  $E_o^2$  in the numerator, and plot  $(E^3/\Upsilon)^{2/5}$  against  $E^2$  (Ref. 7). Figure 7 shows such plots for  $x=0.22$  at various temperatures. The linearity of the plots and their extrapolations (which converge toward reasonable values of  $E_o$  at large  $E$ ) indicate that the excitonic transitions indeed play the dominant role in the Voigt effect of DMS alloys. Some deviation from the linearity of such a curve was noticeable at higher temperatures and/or for  $x \leq 0.13$  or  $x \geq 0.41$ . Such a deviation appears to arise from the larger error in the determination of the Voigt effect,

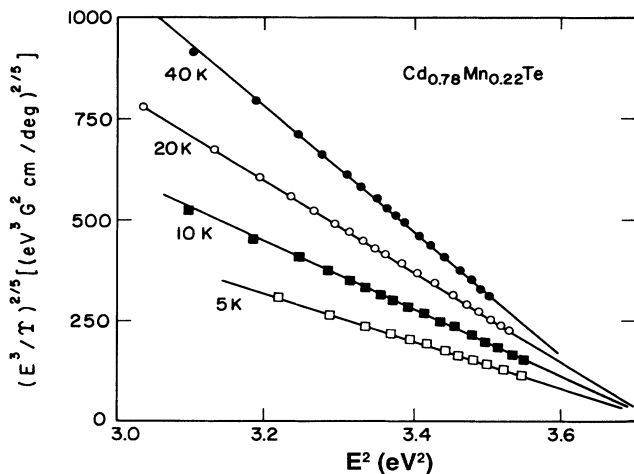


FIG. 7.  $(E^3/\Upsilon)^{2/5}$  vs  $E^2$  for  $\text{Cd}_{1-x}\text{Mn}_x\text{Te}$ ,  $x=0.22$  at several temperatures ( $T=5, 10, 20$ , and  $40$  K), where  $E$  is the photon energy. This plot demonstrates the photon-energy dependence of the Voigt effect according to an excitonic model, Eq. (6).

TABLE I. Temperature dependence of  $E_o$  and  $m^{5/4}$  in  $\text{Cd}_{1-x}\text{Mn}_x\text{Te}$ . The unit for  $m^{5/4}$  is  $(\text{G cm}^{1/2})/(\text{eV deg}^{1/2})$ .

$x$	$T$ (K)	$E_o$ (eV)	$m^{5/4}$
0.22	5	1.937	2 789
	10	1.934	4 361
	20	1.931	6 546
	40	1.925	9 475
	80	1.909	13 255
0.35	160	1.880	18 446
	5	2.147	4 594
	10	2.146	5 613
	20	2.143	6 911
	40	2.133	9 000
	80	2.106	11 884
	160	2.074	13 811

which is smaller at these temperatures and Mn concentrations.

In Table I we show  $E_o$  and  $m^{5/4}$ ,  $E_o^2$  and  $m$  being, respectively, the intercept on the horizontal axis and the slope of the linear fits such as those shown in Fig. 7. Since the Voigt effect is inversely proportional to  $m^{5/2}$ ,  $m^{5/4}$  is proportional to the  $M^{-1}$ . A plot of  $m^{5/4}$  versus  $T$  thus shows the temperature dependence of inverse magnetic susceptibility. At the higher temperatures the magnetization follows a Curie-Weiss law, but deviates from it at the lower temperatures. A similar behavior was obtained from Faraday effect measurements (see Fig. 7 in Ref. 6). We note that the Voigt effect for  $x=0.31$  is larger than that for  $x=0.22$  for  $T \geq 40$  K, but smaller for  $T \leq 20$  K, for the reasons associated with Mn-Mn antiferromagnetic interactions discussed earlier in this section.

### B. $\text{Cd}_{1-x}\text{Mn}_x\text{Se}$

Three different Voigt geometries employed in  $\text{Cd}_{1-x}\text{Mn}_x\text{Se}$  are shown in Fig. 8: (i)  $\mathbf{H} \parallel \hat{c}$ ,  $\mathbf{k} \perp \hat{c}$ , (ii)  $\mathbf{H} \perp \hat{c}$ ,  $\mathbf{k} \parallel \hat{c}$ , and (iii)  $\mathbf{H} \perp \hat{c}$ ,  $\mathbf{k} \perp \hat{c}$ . In this section, we discuss the anisotropy of the Voigt effect revealed in the experimental results based on these geometries.

The experimental results for case (i) are displayed in

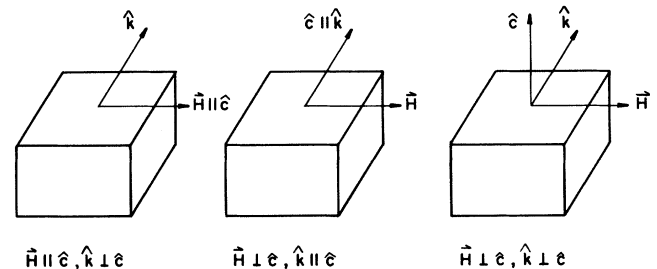


FIG. 8. Three Voigt geometries for a uniaxial (wurtzite) crystal such as  $\text{Cd}_{1-x}\text{Mn}_x\text{Se}$ .

Fig. 9. The transmission of  $\text{Cd}_{1-x}\text{Mn}_x\text{Se}$ ,  $x=0.31$ ,  $T=20$  K,  $l=4.32$  mm with the polarizer and analyzer oriented at  $+45^\circ$  and  $-45^\circ$  with respect to the  $\hat{c}$  axis, respectively, was recorded as a function of photon energy. The curve shown in Fig. 9(a) is for zero magnetic field, and the observed oscillations are due to the intrinsic birefringence. (Note that this effect is totally absent in cubic samples, such as  $\text{Cd}_{1-x}\text{Mn}_x\text{Te}$ .) The intensity minima (maxima) correspond to  $\delta=(2\pi l/\lambda)(n_e-n_o)=2\pi p[\pi(2p+1)]$ , where  $\delta$  is the phase difference between the two "normal modes," one parallel and the other perpendicular to the  $\hat{c}$  axis,  $n_e$  and  $n_o$  are the refractive indices for each "normal mode," and  $p$  is an integer. The lower spectrum [Fig. 9(b)] is for  $H=60$  kG (applied  $\parallel\hat{c}$ ), where the *shift* of the oscillation pattern represents the Voigt effect in this configuration. As has been discussed in an earlier publication,<sup>8</sup> below a certain frequency the intrinsic birefringence ( $n_e-n_o$ ) increases with increasing photon energy but starts decreasing above that (labeled "turning point" in Ref. 8), i.e., the corresponding  $p$  values decrease with increasing wave number (see Fig. 6 in Ref. 8). For the sample and the temperature corresponding to Fig. 9, this "turning point" is around  $16000$   $\text{cm}^{-1}$ . Since the natural birefringence or the value of  $p$  decreases with increasing wave number in the spectral range shown in Fig. 9, the shorter periods between the oscillations at  $H=60$  kG than at  $H=0$  is an indication that the superposition of the intrinsic birefringence and that due to the Voigt effect *decreases more rapidly* with increasing wave number than the intrinsic birefringence by itself. In other words, the total birefringence (observed at  $H\neq 0$ ) is *less*

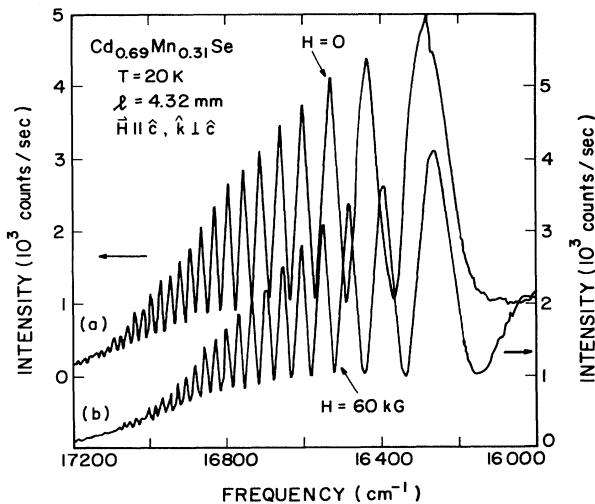


FIG. 9. A channeled spectrum in the radiation transmitted by  $\text{Cd}_{1-x}\text{Mn}_x\text{Se}$ ,  $x=0.31$ ,  $T=5$  K,  $\mathbf{k}\perp\hat{c}$ ,  $H=0$  (a) and  $\mathbf{H}\parallel\hat{c}$  with  $H=60$  kG (b), the sample being placed between two crossed polarizers making a  $\pm 45^\circ$  angle with respect to  $\hat{c}$ . The upper spectrum involves the intrinsic birefringence, whereas in the lower spectrum the total birefringence includes both intrinsic and magnetic-field-induced birefringence, i.e., the Voigt effect. In this spectral range, the intrinsic birefringence *decreases* with increasing photon energy (see Fig. 6 in Ref. 8).

than the intrinsic birefringence (observed at  $H=0$ ). The absolute value of the Voigt effect  $\phi$  was obtained by recording the transmitted intensity while the magnetic field was increased from 0 to 60 kG (similar to the curve in Fig. 2) at several wavelengths. At  $16300$   $\text{cm}^{-1}$ ,  $\phi$  is about  $2\pi$  and increases at higher frequencies. In this configuration ( $\mathbf{H}\parallel\hat{c}$ ,  $\mathbf{k}\perp\hat{c}$ ), the Voigt effect is found to be the largest, a consequence of the larger Zeeman shift of the  $A$  exciton in  $\mathbf{H}\parallel\hat{c}$ . (Note that this is the only configuration with  $\mathbf{H}\parallel\hat{c}$ .) In Table II, we show  $(\phi/2\pi)$  due to the Voigt effect alone (i.e., after subtracting the natural birefringence from the total birefringence when  $\mathbf{k}\perp\hat{c}$ ).

Figure 10 shows the transmission curve observed in  $\text{Cd}_{1-x}\text{Mn}_x\text{Se}$ ,  $x=0.31$ ,  $T=5$  K,  $H=60$  kG,  $l=5.60$  mm for  $\mathbf{H}\perp\hat{c}$ ,  $\mathbf{k}\parallel\hat{c}$ , case (ii), where its intrinsic birefringence does not come into play. Again, each successive maximum or minimum corresponds to an additional increase or decrease of  $\phi$  by  $2\pi$ . The absolute value of  $\phi$  at  $16600$   $\text{cm}^{-1}$  and  $H=60$  kG is  $5\pi$ . In general, the Voigt effect for  $\mathbf{H}\perp\hat{c}$ ,  $\mathbf{k}\parallel\hat{c}$  is smaller than for  $\mathbf{H}\parallel\hat{c}$ ,  $\mathbf{k}\perp\hat{c}$  and larger than for  $\mathbf{H}\perp\hat{c}$ ,  $\mathbf{k}\perp\hat{c}$ , case (iii), where no significant change in phase with magnetic field is observed (see Table II).

The explanation of the striking anisotropy of the Voigt effect in  $\text{Cd}_{1-x}\text{Mn}_x\text{Se}$  has to be sought in the differences in the Zeeman splittings of the excitons for  $\mathbf{H}\parallel\hat{c}$  [Fig. 3(b)] and  $\mathbf{H}\perp\hat{c}$  [Fig. 3(c)] in conjunction with the selection rules.<sup>9</sup> The conduction-band minimum of  $\text{Cd}_{1-x}\text{Mn}_x\text{Se}$  is at the zone center with  $\Gamma_7$  symmetry. The valence-band maximum, also at the zone center, has  $\Gamma_9$  symmetry and is separated from the next-lower-lying  $\Gamma_7$  maximum by the crystal-field splitting. The excitons associated with  $\Gamma_9$  and  $\Gamma_7$  are labeled  $A$  and  $B$ , respectively. The  $A$ -excitonic transition is allowed only for  $\mathbf{E}\perp\hat{c}$  whereas the  $B$ -excitonic transition is observed with  $\mathbf{E}\parallel\hat{c}$  as well as  $\mathbf{E}\perp\hat{c}$ , where  $\mathbf{E}$  is the electric vector of the light.<sup>10</sup>

When the magnetic field is applied along the optic axis

TABLE II. Comparison of Voigt effect in  $\text{Cd}_{1-x}\text{Mn}_x\text{Se}$  at  $H=60$  kG for the three different geometries in Fig. 8.

$x$	$T$ (K)	$E$ ( $\text{cm}^{-1}$ )	$\phi/2\pi$		
			$\mathbf{H}\parallel\hat{c}$ , $\mathbf{k}\perp\hat{c}$	$\mathbf{H}\perp\hat{c}$ , $\mathbf{k}\parallel\hat{c}$	$\mathbf{H}\perp\hat{c}$ , $\mathbf{k}\perp\hat{c}$
			$l=3.72$ mm	$l=3.03$ mm	$l=3.72$ mm
0.26	5	16000	5.0	1.5	<0.2
		16250	8.4	2.5	<0.2
		16500	15.6	4.85	<0.5
		16600	21.0	6.6	<0.5
		16700	29.0	8.8	<0.5
			$l=4.32$ mm	$l=5.60$ mm	$l=4.32$ mm
0.31	5	15500	0.75	0.5	<0.2
		16200	2.0	1.3	<0.2
		16600	4.3	2.5	<0.5
0.31	20	16350	1.2	0.8	<0.1
		16500	1.6	1.0	<0.1
		16600	2.0	1.4	<0.1
		16700	2.35	1.6	<0.1

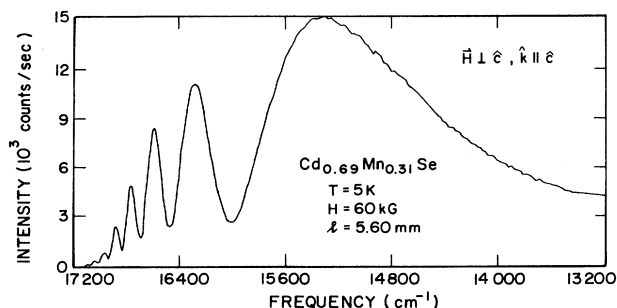


FIG. 10. The transmission curve for  $\text{Cd}_{1-x}\text{Mn}_x\text{Se}$ ,  $x=0.31$ ,  $T=5\text{ K}$ ,  $\mathbf{H}\perp\hat{c}$ ,  $\mathbf{k}\parallel\hat{c}$ ,  $H=60\text{ kG}$ , i.e., in a configuration in which the intrinsic birefringence is absent.

( $\hat{c}$ ) [Fig. 3(b)], two  $\hat{\sigma}_{\pm}$  transitions originate from  $\Gamma_9(A)$  (labeled 1,6) and two  $\hat{\sigma}_{\pm}$  (labeled 3, 4) and two  $\hat{\pi}$  transitions (labeled 2, 5) originate from  $\Gamma_7(B)$ , all terminating at the  $\Gamma_7$  conduction band. Since the Zeeman splitting of the  $A$  exciton is larger and the  $A$ -excitonic transition level lies closer to the photon energies where the Voigt effect is studied,  $n_{\sigma}$  experiences a stronger dispersive effect in the presence of an external magnetic field than does  $n_{\pi}$ . Without an external magnetic field, the extraordinary refractive index,  $n_e$  is larger than the ordinary refractive index,  $n_o$  (Ref. 8). For  $\mathbf{H}\parallel\hat{c}$ ,  $n_o$  (or  $n_e$ ) becomes larger with increasing magnetic field, resulting in a smaller total birefringence.

If the magnetic field is applied *perpendicular* to  $\hat{c}$  [Fig. 3(c)], the eigenstates are admixtures of different ( $j, j_z$ ) states, where  $j$  and  $j_z$  correspond to total angular momentum and its  $z$  component, respectively. For  $\mathbf{H}\perp\hat{c}$ , we choose the  $z$  axis along  $\mathbf{H}$ . In the limit of zero magnetic field, each eigenstate is an equal admixture of  $+j_z$  and  $-j_z$  although it would have had a definite value of  $j_z$  had we chosen  $\hat{z}$  along  $\hat{c}$ . With increasing magnetic field, each eigenstate will become close to an eigenstate of ( $j, j_z$ ) and the transitions labeled 1,3,4,6 will be increasingly polarized in a plane perpendicular to  $\mathbf{H}$ , whereas those for 2,5 will be polarized parallel to  $\mathbf{H}$ . (Although transitions other than 1–6 are allowed for  $\mathbf{H}\perp\hat{c}$ , we assume here that only 1–6 play a dominant role.) These considerations can enable us to interpret the difference in the Voigt effect for  $\mathbf{H}\perp\hat{c}$ ,  $\mathbf{k}\parallel\hat{c}$ , and for  $\mathbf{H}\perp\hat{c}$ ,  $\mathbf{k}\perp\hat{c}$ .

As mentioned earlier,  $A$ -excitonic transition is allowed only for  $\mathbf{E}\perp\hat{c}$  at  $H=0$ . For  $\mathbf{H}\perp\hat{c}$ ,  $\mathbf{k}\parallel\hat{c}$ , case (ii) in Fig. 8, the 1 and 6 transitions contribute to  $n_{\perp}$  because  $\mathbf{E}$  is  $\perp\hat{c}$ , assuming that the same selection rule applies for  $H\neq 0$ . The transitions 3 and 4, associated with the  $B$  exciton, will also contribute to  $n_{\perp}$  in this configuration, but their contribution to the Voigt effect will be more or less can-

celled by the contribution to  $n_{\parallel}$  from the 2 and 5 transitions. As discussed above, for  $\mathbf{H}\perp\hat{c}$ ,  $\mathbf{k}\perp\hat{c}$ , case (iii),  $\mathbf{E}$  associated with the 1, 3, 4, and 6 transitions is perpendicular to  $\mathbf{H}$ , but only 3 and 4 can be polarized parallel to  $\hat{c}$  since the  $A$  exciton appears only for  $\mathbf{E}\perp\hat{c}$ . Once more, the effects of 2 and 5 will compensate those from 3 and 4. Thus the negligible Voigt effect for  $\mathbf{H}\perp\hat{c}$ ,  $\mathbf{k}\perp\hat{c}$  can be understood.

To summarize: for  $\mathbf{H}\parallel\hat{c}$ , the excitonic Zeeman splittings of  $\text{Cd}_{1-x}\text{Mn}_x\text{Se}$  are similar to those for  $\text{Cd}_{1-x}\text{Mn}_x\text{Te}$  and the Voigt effect is the largest among the three configurations displayed in Fig. 8. The Zeeman splitting of the  $A$  exciton for  $\mathbf{H}\perp\hat{c}$  is significantly smaller than that for  $\mathbf{H}\parallel\hat{c}$  and the Voigt effect is correspondingly smaller. In  $\mathbf{H}\perp\hat{c}$ ,  $\mathbf{k}\perp\hat{c}$ , where the  $A$  exciton should play an insignificant role, the Voigt effect is negligible.

## V. CONCLUDING REMARKS

The Voigt effect is a magneto-optic phenomenon second order in  $H$  and is usually very difficult to observe at laboratory magnetic fields. However, the birefringence due to the Voigt effect in diluted magnetic semiconductors for photon energies near the band gap at  $H=60\text{ kG}$  is of the order of the natural birefringence of calcite in the visible range. This giant Voigt effect is due to the huge excitonic Zeeman splitting and exhibits a quadratic dependence on the magnetization ( $M$ ). If, say, the Zeeman splitting in  $\text{Cd}_{1-x}\text{Mn}_x\text{Te}$ ,  $x=0.25$ , is 100 times larger than in  $\text{Cd}_{1-x}\text{Mn}_x\text{Te}$ ,  $x=0.02$ , the Voigt effect in the former will be 10 000 times larger than in the latter. It must be emphasized that even in DMS alloys the Voigt effect is readily observed only at low temperatures and at high magnetic fields. For example, if  $\phi$  is  $10\,000^\circ$  for  $\text{Cd}_{1-x}\text{Mn}_x\text{Te}$ ,  $x=0.3$ , at  $20\text{ K}$  and  $60\text{ kG}$ , it will be only  $1^\circ$  at  $300\text{ K}$  and  $6\text{ kG}$  at photon energies corresponding to the same  $E/E_0$ , assuming the magnetic susceptibility at  $300\text{ K}$  is 10 times smaller than at  $20\text{ K}$ .

In contrast to the Voigt effect in the cubic  $\text{Cd}_{1-x}\text{Mn}_x\text{Te}$ , a strong anisotropy was observed in the Voigt effect in  $\text{Cd}_{1-x}\text{Mn}_x\text{Se}$ . For  $\mathbf{k}\parallel\hat{c}$ , the Voigt effect can be measured directly as in  $\text{Cd}_{1-x}\text{Mn}_x\text{Te}$ , whereas for  $\mathbf{k}\perp\hat{c}$  the intrinsic birefringence has to be subtracted off from the total birefringence. In the case of  $\mathbf{H}\parallel\hat{c}$ ,  $\mathbf{k}\perp\hat{c}$ , where the Voigt effect is the largest among the three basic experimental geometries, the Voigt effect reduces the total birefringence near the absorption edge.

## ACKNOWLEDGMENT

The work reported in this paper was supported by National Science Foundation Grant No. DMR-89-13706.

\*Present address: Texas Instruments Inc., Dallas, TX 75243.

<sup>1</sup>W. Voigt, Ann. Phys. (Leipzig) **1**, 389 (1900).

<sup>2</sup>II-VI diluted magnetic semiconductors are alloys in which the group-II element of a II-VI crystal is in part replaced by a

transition metal, e.g.,  $\text{Mn}^{2+}$ . For an overview, see J. K. Furdyna, J. Appl. Phys. **64**, R29 (1988).

<sup>3</sup>J. A. Gaj, R. R. Galazka, and M. Nawrocki, Solid State Commun. **25**, 193 (1978).

- <sup>4</sup>J. A. Gaj, J. Ginter, and R. R. Galazka, *Phys. Status Solidi B* **89**, 655 (1978).
- <sup>5</sup>D. U. Bartholomew, J. K. Furdyna, and A. K. Ramdas, *Phys. Rev. B* **34**, 6943 (1986).
- <sup>6</sup>Eunsoon Oh, D. U. Bartholomew, A. K. Ramdas, J. K. Furdyna, and U. Debska, *Phys. Rev. B* **38**, 13 183 (1988).
- <sup>7</sup>The  $E_o^2$  in the numerator of Eq. (6) can be included in an iterative fashion. Such an iteration shows that the inclusion of the term results in a change in the value of  $E_o$  by not more than 3 meV. Defining the slopes of the plots of  $(E^3/\Upsilon)^{2/5}$  versus  $(E_o^2 - E^2)$  and  $[E(3E^2 + E_o^2)/\Upsilon]^{2/5}$  versus  $(E_o^2 - E^2)$  by  $m$  and  $m'$ , respectively, we find that  $m'^{5/4}$  is larger than  $m^{5/4}$  by 15%. This is consistent with  $m'^{5/4} \approx (\frac{4}{3})^{1/2} m^{5/4}$  expected for  $E \approx E_o$ .
- <sup>8</sup>Eunsoon Oh, D. U. Bartholomew, A. K. Ramdas, J. K. Furdyna, and U. Debska, *Phys. Rev. B* **42**, 5201 (1990).
- <sup>9</sup>R. L. Aggarwal, S. N. Jaspersen, J. Stankiewicz, Y. Shapira, S. Foner, B. Khazai, and A. Wold, *Phys. Rev. B* **28**, 6907 (1983).
- <sup>10</sup>D. Dutton, *Phys. Rev.* **112**, 785 (1958); D. G. Thomas and J. J. Hopfield, *ibid.* **116**, 573 (1959).